Theor Chem Acc (1998) 100:36–50
DOI 10.1007/s002149800m60

Theoretical
Chemistry Accounts

Regular article

Diatomic potential well depths from analyses of high-resolution electron energy spectra for autoionizing collision complexes*

H. Hotop, T.E. Roth, M.-W. Ruf, A.J. Yencha**

Fachhereich Physik, Universität Kaiserslautern, D-67653 Kaiserslautern, Germany

Received: 30 June 1998 / Accepted: 5 August 1998 / Published online: 28 October 1998

Abstract. High-resolution energy spectra of electrons released in Penning ionization collisions of metastable rare gas atoms Rg*(n*s*) (Rg = He, Ne, Ar, Kr, Xe) with several open-shell and closed-shell atoms are analyzed to determine the well depth of the potential energy curve which describes the respective autoionizing collision complex. We thereby elucidate trends in the chemical interaction of Rg* with closed-shell target atoms A(ns^2) and establish a basis for detailed comparison with the respective interactions involving open-shell, ground state alkali atoms A(*ns*). From electron energy spectra due to associative ionization (RgH^+ formation) in Rg* + H(1*s*) collisions, we determine binding energies for the $RgH^+(^1\Sigma)$ ground state potential (Rg = Ne, Ar, Kr, Xe) with uncertainties around 0.03 eV.

Key words: Autoionizing diatomic collision complexes – Interaction potentials – Metastable rare gas atoms – Penning ionization electron spectroscopy

1 Introduction

The interaction of metastable rare gas atoms (Rg*) with target atomic systems (A) leads to the formation of diatomic collision complexes that may undergo autoionization processes if sufficient energy (electronic and kinetic) is available. The primary results of such processes are the formation of Penning or associative ions by the following reaction schemes [1–4]:

$$\mathrm{Rg^* + A \rightarrow [Rg\text{-}A]^* \rightarrow Rg + A^+ + e^-(\varepsilon)} \quad \text{Penning ionization (PI)} \quad (1a)$$

$$\mathrm{\rightarrow RgA^+ + e^-(\varepsilon)} \quad \text{Associative ionization (AI)} \quad , \quad (1b)$$

where [Rg-A]* represents the collision complex or quasi-molecule. If the excitation energy $E(\mathrm{Rg^*})$ of Rg* exceeds the ionization energy $I(\mathrm{A})$ of A the collision system lies in the ionization continuum of the final $(\mathrm{Rg + A^+}) + \mathrm{e^-}$ states at all internuclear separations R, and autoionization may proceed even in the limit of zero collision energy. The process is resonant in the sense that the emitted electron can take away the excess energy in a way compatible with the Franck-Condon principle. In view of the metastability of the Rg* states considered, the electronic coupling which promotes autoionization is basically of short range; toward large distances, it decreases exponentially in a way which essentially reflects the overlap between the hole in the Rg* atom and the active electron in the target A. Within the electron exchange model for PI [5] the target electron may be viewed to fill the Rg* hole with simultaneous emission of the excited electron in Rg*. As demonstrated in great detail in recent experimental and theoretical work on one of the simplest PI/AI systems [$\mathrm{He^*(2^3S_1) + H(1^2S_{1/2})}$] [6, 7], the process can be very well described by local complex potential theory within the framework of the Born-Oppenheimer approximation, as long as the electron energy is sufficiently large. Within this theory [7–10] the entrance channel $\mathrm{Rg^* + A}$ is described by two (real) local (i.e., only R dependent) functions $V^*(R)$ and $\Gamma(R)$, which form the local complex potential $V_{\mathrm{LCP}}(R) = V^*(R) - i\Gamma(R)/2$. The imaginary part of this complex potential introduces the decay of the entrance channel into the final continuum states. The heavy-particle motion in the exit channel is controlled by the (real) potential $V^+(R)$. Depending

* Dedicated to Prof. Dr. Wilfried Meyer on the occasion of his 60th birthday

** *Permanent address*: Department of Chemistry, State University of New York at Albany, Albany, NY 12222, USA

Correspondence to: H. Hotop
e-mail: hotop@physik.uni-kl.de

on the value of the electron energy ε, the heavy-particle motion in the final state lies in the continuum (Eq. 1a) or it corresponds to the formation of bound RgA^+ levels (Eq. 1b). The two situations are energetically characterized by the criteria:

$$\text{PI}: \quad \varepsilon < E_0 + E_{\text{rel}} \tag{2a}$$

$$\text{AI}: \quad \varepsilon \geq E_0 + E_{\text{rel}}, \tag{2b}$$

where E_0 denotes the asymptotic energy difference (subsequently referred to as nominal energy) between the potential curves V^* and V^+, i.e., $E_0 = V^*(\infty) - V^+(\infty) = E(\text{Rg}^*) - I(\text{A})$; E_{rel} represents the relative collision energy in the entrance channel. Considerable information can be gained about these autoionizing processes from analyses of the electron spectra with respect to the kinetic energy of the electron and the shape of the observed peak structure [1–7, 11– 16]. In particular, one can gain rather direct information on the shape and depth of the incoming and outgoing interaction potentials, $V^*(R)$ and $V^+(R)$, respectively, and – with the aid of model calculations of the energy spectra – on the coupling width $\Gamma(R)$ which is connected with the local transition rate $W(R)$ for spontaneous ionization by $\Gamma(R) = \hbar W(R)$.

Over the past 15 years or so we have conducted systematic electron spectrometric studies of a large number of excited diatomic collision systems [6, 15–26]. For detailed interpretation of these experimental data close collaboration with the group of Wilfried Meyer proved to be crucial and highly beneficial. Through the group's continued efforts, most notably by Mladen Movre and Wilfried Meyer himself, accurate ab initio potential curves became available for several basic PI systems: $\text{He}^*(2^3\text{S}_1, 2^1\text{S}_0) + \text{H}(1^2\text{S}_{1/2})$, $\text{D}(1^2\text{S}_{1/2})$, $\text{Li}(2^2\text{S}_{1/2})$, $\text{Na}(3^2\text{S}_{1/2})$, $\text{He}^*(2^3\text{S}_1)$, and $\text{Ca}(4^1\text{S}_0)$, including local autoionization width functions [6, 7, 15, 18, 21, 25]. Based on these (complex) potentials, scattering calculations for the relevant experimental observables were carried out; through detailed comparison of theoretically predicted with experimentally measured quantities, most notably (angle-dependent) electron energy spectra, substantial insight was gained into the autoionization dynamics in these systems [6, 7, 15, 18, 21, 22, 25, 26]. This insight will guide us in future work.

The purpose of this paper is to summarize our present knowledge on the chemical interactions of Rg* with several prototype open- and closed-shell atoms, A, as gained from analysis of measured high-resolution electron energy spectra for the respective autoionizing collision system. Moreover, we dwell on the protonated systems RgH^+ (Rg = Ne–Xe) for which we determine potential well depths from electron spectra due to AI in Rg* + H collisions. In Sect. 2 we discuss the theoretical framework for the interpretation of electron energy spectra due to PI and AI processes. A brief description of a typical experimental setup used to measure high-resolution electron spectra for the Rg*-A system is presented in Sect. 3. In Sect. 4 we discuss in some detail the interaction of Rg* with closed-shell target atoms (Mg, Ca, Sr, Ba, Yb, Hg) and with open-shell target atoms (H, D, Li, Na, K, Rb, Cs). Well depths for the $\text{RgH}^+(\text{X}^1\Sigma)$ potentials through analysis of AI electron spectra for the respective Rg*+H systems are also described in Sect. 4.

2 Theoretical framework for the determination of potential well depths from electron energy spectra due to autoionizing collision complexes

The PI/AI process within the potential curve model which is based on the Born-Oppenheimer approximation and the Franck-Condon principle for the electronic transition is characterized in Fig. 1. The upper curve represents the incoming neutral potential energy curve for the diatomic collision system $Rg^* + \text{A}$ of relative collision energy E_{rel} with formation of the quasi-molecule (Rg-A)*, of well depth D_e^* at R_e^*, from which autoionization may occur over a range of internuclear distances R. The point R_t^* indicates the classical turning point in the collision system for zero impact parameter b. The middle curve represents the outgoing ionic potential energy curve of the collision system with a well depth for the molecular ion of D_e^+ (somewhat exaggerated for most Penning-type systems except for $\text{A}^+ = \text{H}^+$) at R_e^+. The lower curve represents the difference potential $V^* - V^+$ as a function of R with a minimum at R_m. Note that the value of R_m is shifted to a slightly larger value than R_e^* due to the attractiveness in the ionic channel. The dashed curve associated with the difference potential is a typical autoionization width function $\Gamma(R)$. Also shown to the right of the difference potential curve is a hypothetical electron energy spectrum $P(\varepsilon)$ with contributions from PI (open area) and AI (hatch area). E_0 in Fig. 1 is given by $E_0 = V^*(\infty) - V^+(\infty)$, i.e., the

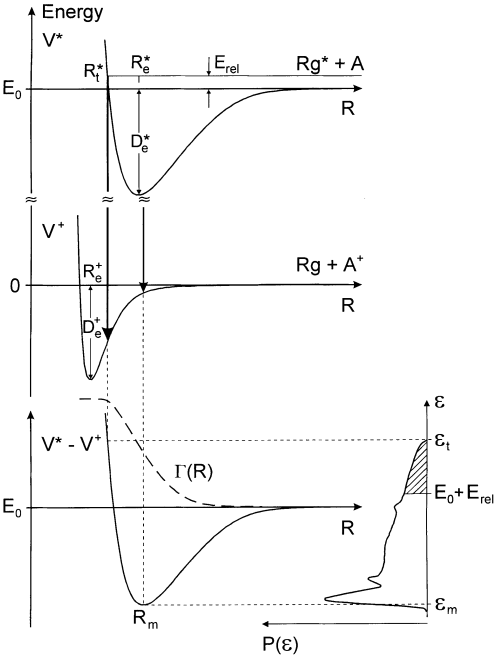

Fig. 1. Two-state potential energy curve model for Penning ionization (PI) and associative ionization (AI) in metastable rare gas atom (Rg*)-atomic (A) collision systems

energy of the difference potential at infinite internuclear distance, which is referred to as the "nominal" energy difference. Also shown on the electron spectrum is the 44% point of the low-energy "edge" given by ε_m from which the well depth D_e^* can be deduced using Eq. (6) in conjunction with reasonable estimates of the potential difference $[V^+(\infty) - V^+(R_e^*)]$ (see below). The point ε_t in the electron spectrum represents the maximum electron energy possible for transitions occurring at the classical turning point R_t^*.

A key quantity for the explanation and interpretation of the electron energy spectrum $P(\varepsilon)$ resulting from PI/AI is the (local) difference potential function $[V^*(R) - V^+(R)]$. If we assume that the positions and momenta of the heavy particles are frozen during autoionization occurring at internuclear distance R (classical Franck-Condon principle), depicted by the vertical heavy arrows in Fig. 1, the energy of the emitted electron is simply given by the difference potential, i.e., we have:

$$\varepsilon(R) = V^*(R) - V^+(R) \tag{3}$$

Note that this equation is independent of the actual impact parameter b or, equivalently, of the orbital angular momentum J^* of the collision system, since we assumed the radial and angular motion of the nuclei to be frozen in the electron emission process. Therefore, the orbital angular momentum J^+ and the centrifugal potential in the exit channel are the same as the corresponding quantities in the entrance channel, and the centrifugal potentials cancel in the difference potential. This approximation is equivalent to assuming that the ejected electron does not carry away angular momentum and therefore leaves as an s-wave. Classical estimates [18, 26] for the expected angular momentum exchange between the heavy-particle system and the emitted electron show that higher electron partial waves l may in fact be present, but are typically restricted to values $l \leq 3$ [6, 7, 18, 26]. Angular momentum exchanging processes lead to some spectral broadening and angle-dependent shifts, as first observed for $He^*(2^3S) + Li(2\,^2S)$ [26]. Theoretical calculations for the systems $He^*(2^3S) + H$, Li showed that electron spectra measured at an angle $\Theta = 90^\circ$ (relative to the collision velocity direction) are to a large extent representative for angular-integrated spectra in agreement with experimental observations [6, 7, 18]. The following discussion exclusively addresses electron spectra measured at $\Theta = 90^\circ$.

The situation depicted in Fig. 1 is quite typical for PI systems involving Rg* and A with substantial mutual long-range attraction. The (average) thermal collision energy (typically $E_{rel} = 50$ meV) is smaller than the well depth $D_e^* = V^*(R_e^*)$ of the entrance channel potential (several tenths of an eV). In view of the closed-shell nature of the ground state Rg atoms the ionic exit channel potential for the Rg-A^+ system is in general only weakly bound by polarization forces which, however, rise substantially from Rg = He to Xe. As is obvious from Fig. 1, AI can only occur if the autoionization process happens at internuclear distances close to the classical turning point R_t^* in $V^*(R)$ for which the energy condition Eq. (2b) holds and the highest energies in the spectrum $P(\varepsilon)$ are obtained. In contrast, the lowest energies originate from electron emission at distances around R_m, which denotes the minimum point of the difference potential; for the situation depicted in Fig. 1, R_m is quite close to R_e^*. In view of the relationship $P(\varepsilon)d\varepsilon = P(R)dR$, where $P(R)$ represents the radial probability density for electron emission in the interval $(R, R + dR)$, the electron spectrum $P(\varepsilon) = P(R)/|d\varepsilon/dR|$ exhibits a classical, integrable singularity at the point $R = R_m$, where the difference potential $\varepsilon(R)$ is stationary [9, 27]. In a semiclassical description the singularity is replaced by the square of an Airy function [9, 28] in the region where the quadratic expansion $\varepsilon(R) = \varepsilon_m + \varepsilon''(R_m)(R - R_m)^2/2$ around the minimum point R_m is valid. For sufficiently low ionization probability and weak variation of $\Gamma(R)$ in the neighborhood of R_m, the contribution $P_{J^*}(\varepsilon)$ of each entrance channel partial wave J^* to the electron spectrum around ε_m is explicitly given by [9, 28, 29]:

$$P_{J^*}(\varepsilon) = [2\pi\Gamma(R_m)/\hbar u_{J^*}(R_m)] \times [\hbar u_{J^*}(R_m)\varepsilon''(R_m)^2/4]^{-1/3} Ai^2(z) \tag{4}$$

where $u_{J^*}(R_m)$ denotes the radial collision velocity for the partial wave J^* at $R = R_m$ and $Ai(z)$ represents an Airy function with argument $z = [2/\varepsilon''(R_m)]^{1/3}\,[1/\hbar u_{J^*}(R_m)]^{2/3}(\varepsilon_m - \varepsilon)$. The corresponding peak in $P_{J^*}(\varepsilon)$ has a width which is related to the curvature of the difference potential $\varepsilon''(R) = d^2\varepsilon/dR^2$ at the distance R_m and to the radial velocity of the collision system in this region. We note that improved semiclassical dezscriptions [28, 30], e.g., by taking into account the variation of $\Gamma(R)$ around R_m [28], do not lead to substantial changes as long as the discussion is confined to the main Airy peak. When a sufficiently large number of orbital angular momenta contribute to autoionization around R_m, the semiclassical expression for the main Airy peak is very similar to the result of exact quantum mechanical calculations [30]. Analysis of the $Ai^2(z)$ function in Eq. (4) shows that the value ε_m of the classical minimum of the electron energy occurs at the 44% intensity point on the low-energy side (edge [9]) of the main Airy peak. This statement is also valid to a good approximation for the full spectrum $P(\varepsilon)$ as well as for quantum mechanical results. This simple 44% criterion is used to extract the entrance channel well depth D_e^* from the experimentally determined value for $E_0 - \varepsilon_m$, as described below.

To illustrate the appearance of realistic electron spectra for systems with substantial entrance channel well depths and weak attraction in the ionic exit channel we present the results of quantum mechanical calculations for the electron spectra of the reactions $He^*(2^3S, 2^1S) + Ca \rightarrow He + Ca^+(4s) + e^-$ [15] in Fig. 2. The spectra were obtained with an appropriate average over the collision energy distribution. The effect of resolution on the appearance of the electron energy spectrum is demonstrated by the full lines, which are obtained after convolution of the pure theoretical spectra (dashed lines) with a Gaussian spectrometer function (60 meV FWHM). What is of importance in connection

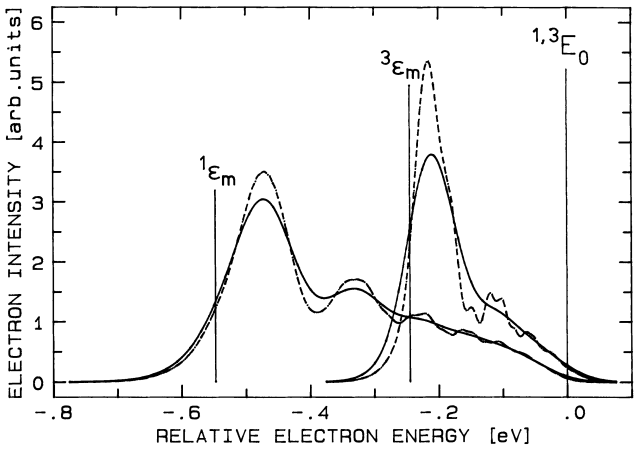

Fig. 2. Theoretical electron energy spectra for the reactions $He^*(2^3S, 2^1S) + Ca \rightarrow He + Ca^+(4s\,^2S_{1/2}) + e^-$, as calculated for the experimental distribution of collision energies before (*dashed lines*) and after convolution (*full lines*) with the experimental electron energy resolution (60 meV FWHM). The spectral areas correspond to the respective cross sections for $Ca^+(4s\,^2S_{1/2})$ formation (2^3S:2^1S ratio 0.64). The electron energies are relative to the respective nominal energies $^{3,1}E_0$ for $Ca^+(4s\,^2S_{1/2})$ formation [$^{3,1}E_0$ = excitation energy of $He^*(2^{3,1}S)$ minus the ionization potential (IP) of Ca]

with the present paper is the location of the low-energy edge. In the theoretical spectra (dashed lines) the position of the edge ε_m corresponds to the 35% $[He^*(2^1S) + Ca]$ and to the 43% $[He^*(2^3S) + Ca]$ intensity points on the low-energy side of the main Airy peak. After convolution, the ε_m positions appear at a point of higher intensity, and this effect has to be taken into account in the proper evaluation of experimental Airy peak structure [15, 16, 29].

In order to deduce the entrance channel well depth D_e^* from the experimentally measured edge position ε_m for situations similar to those depicted in Fig. 1 we proceed as follows. To a first approximation the distance R_m, at which the difference potential attains its minimum, can be set equal to R_e^*; this is especially true for systems with weak attraction in the ionic potential $V^+(R)$, including the important case Rg = He and also Rg = Ne. We then obtain a simple equation to extract the well depth $D_e^* \equiv V^*(R_e)$ from the experimentally measured edge position ε_m as follows:

$$\begin{aligned} \varepsilon_m &= V^*(R_m) - V^+(R_m) \approx V^*(R_e^*) - V^+(R_e^*) \\ &= E_0 - D_e^* - [V^+(R_e^*) - V^+(\infty)], \end{aligned} \tag{5}$$

and therefore,

$$D_e^* \approx E_0 - \varepsilon_m + [V^+(\infty) - V^+(R_e^*)]. \tag{6}$$

We use this equation in conjunction with reasonable estimates for $[V^+(R_e^*) - V^+(\infty)]$ to determine well depths for the interaction potentials of He^* atoms with alkali, alkaline earth, Yb, and Hg atoms. This approach is also a good approximation for extracting well depths of the $Ne^* + A$ systems. For the heavier Ar*, Kr*, and Xe* atoms a more detailed procedure must be used [19]. Note that the value for R_e^* in Eq. (6) is in general not known, but it can be estimated with reference to chemically similar systems or by, for example, the sum of the atomic radii of Rg^* and A. Even if R_e^* is not well-known, however, the well depth D_e^* can still be determined quite accurately as long as the interaction in $V^+(R)$ is small in the relevant range of internuclear distances.

3 Experimental methods

A typical experimental setup for studies of electron energy spectra due to PI and AI processes with Rg* is sketched in Fig. 3. It consists of an intense, collimated and (preferably) state-selected projectile beam of Rg*, a suitable target (either in the form of a static diffuse gas or, as shown in Fig. 3, a collimated beam of atoms or molecules), and a high-resolution electron spectrometer. In addition, diagnostic means to characterize the properties of the projectile beam, of the target, and of the electron spectrometer are involved.

We have used a differentially pumped discharge source to produce a Rg* beam with intensities in the range $(2–20) \times 10^{14}$ cm^{-2} s^{-1}, as summarized in a recent publication [31]. For all Rg atoms two metastable states with lifetimes long compared with the time-of-flight from the source to the monitor detector are present in the beam. The energies [32], lifetimes [32], and other properties of the Rg* beams are summarized in Table 1. In the case of He, the $He^*(2^3S)$ and $He^*(2^1S)$ states have sufficient energy to ionize all atoms (except for He and Ne) and molecules. In the case of heavier Rg the two metastable levels are given by $Rg^*[(n-1)p^5\ ns\ ^3P_2]$ and $Rg^*[(n-1)p^5\ ns\ ^3P_0]$ (n = 3–6 for Rg = Ne–Xe). The energy separations between the lower-lying $^3P_2$ and

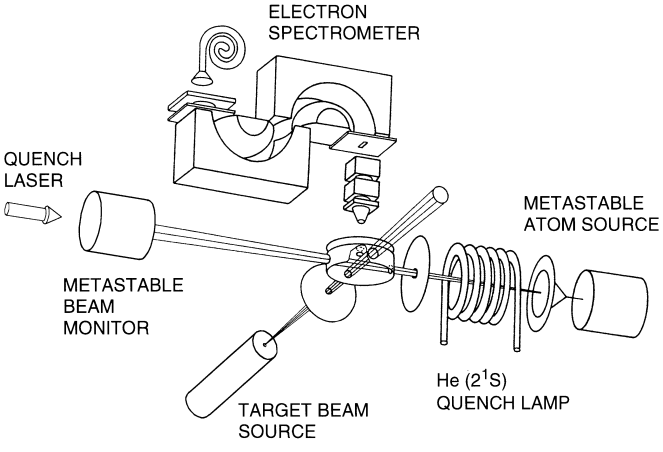

Fig. 3. Schematic representation of a typical crossed-beam apparatus used to obtain electron spectra at 90° to the plane of the interacting, mutually perpendicular *metastable* and *target atomic beams*. For the case where the metastable beam consists of mixed $He^*(2^3S, 2^1S)$ metastables, a *$He^*(2^1S)$ quench lamp* may be used to produce a beam of pure $He^*(2^3S)$ metastables. For the heavier metastable beam systems $Rg^*(ns\,^3P_2, ^3P_0)$ (Rg = Ne, Ar, Kr, Xe) state selection of either component can be accomplished through the use of an appropriate quench laser aligned anticollinearly to the metastable beam

Table 1. Properties of metastable rare gas (Rg*) atoms (data for energies and lifetimes taken from Ref. [32]; for Ref. see [32])

Rg*	Excitation energy (eV)	Lifetime (s)		Average velocity (m s^{-1})[a]	Flux ratio[b]
		Theoretical	Experimental		
He*($2s\,^1S$)	20.6158	0.0195	0.0197		
				2000	6–8
He*($2s\,^3S$)	19.8196	7900	9000		
Ne*($3s\,^3P_0$)	16.7154	430			
				900	5.2(2)
Ne*($3s\,^3P_2$)	16.6191	24.4	> 0.8		
Ar*($4s\,^3P_0$)	11.7232	44.9			
				640	6–7
Ar*($4s\,^3P_2$)	11.5484	55.9	38 (+8, −5)		
Kr*($5s\,^3P_0$)	10.5624	0.49			
				440	10–14
Kr*($5s\,^3P_2$)	9.9152	85.1	39 (+5, −4)		
Xe*($6s\,^3P_0$)	9.4472	0.078	0.128 (+0.122, −0.042)		
				350	30–60
Xe*($6s\,^3P_2$)	8.3153	149.5	42.9 (9)		

[a] $v_{Rg} = 4000(\pm 200)(M_{Rg})^{-1/2}$ m s^{-1}, Ref. [31]
[b] Property depending upon discharge source conditions. He*:$2^3S/2^1S$; Ne*, Ar*, Kr*, Xe*: $^3P_2/^3P_0$ (see Ref. [19, 31, 35, 36–38, 54])

the $^3P_0$ levels increase strongly from Ne to Xe, reflecting the transition from (nearly) LS coupling (Ne) to *jj* coupling (Xe). State selection of He* is simply realized by selective removal of the He*(2^1S) component using optical excitation on the 2^1S-2^1P transition ($\lambda = 2.06$ μm) with light from a He discharge (see Fig. 3) [33]. State selection of heavier Rg* is achieved by selective optical excitation of either component with suitable lasers [34–36]. In recent work, we have advantageously used tunable diode lasers for efficient removal of Rg*($^3P_2$) or Rg*($^3P_0$) (Rg = Ne–Xe) by optical excitation of the state in question on a suitable *ns-np* transition in a special way which turned out to be extremely efficient (quenching efficiencies of 99.9% were observed in favourable cases) [37, 38]. As indicated in Fig. 3, the "quenching" diode laser is directed anticollinearly to the Rg* beam and carefully aligned to provide optimal overlap of the laser and atomic beams. In order to efficiently excite the whole velocity distribution and all possible isotopic and hyperfine components of Rg*, the single-mode diode laser (frequency width typically 30–50 MHz) is rapidly scanned over a frequency range 5–10 GHz at an optimized repetition rate by variation of the diode current. The velocity distribution of Rg* is that of a (mildly) supersonic beam with a velocity width (FWHM) $\Delta v(\mathrm{Rg}^*)/\langle v(\mathrm{Rg}^*)\rangle$ around 30% ($\langle v\rangle$ denotes the average velocity) and an average kinetic energy of $\langle E(\mathrm{Rg}^*)\rangle = 60$–$85$ meV (depending on source conditions [31]). The velocity distributions were measured by time-of-flight techniques or by Doppler-shifted laser-induced fluorescence spectroscopy. The average relative collision energy $\langle E_{\mathrm{rel}}\rangle$ is calculated by an appropriate integral over the normalized velocity distributions of Rg* and A. For crossed Rg* and A beams, it is given, to good approximation, by $\langle E_{\mathrm{rel}}\rangle = (\mu/2)[\langle v(\mathrm{Rg}^*)\rangle^2 + \langle v(\mathrm{A})\rangle^2]$ [μ = reduced mass $= m_{\mathrm{Rg}} m_{\mathrm{A}}/(m_{\mathrm{Rg}} + m_{\mathrm{A}})$]. The absolute fluxes of the different Rg* species (see Table 1) are determined with a detector (beam monitor) which involves electron emission induced by impact of Rg* at a calibrated conducting surface [32]. The ratio of the fluxes for the two respective metastable states for each Rg (relevant for the conditions of our discharge source) has been determined as given in Table 1 [31, 36, 37, 38].

For the experimental results presented in this paper three different electron spectrometers were used: namely a single-stage cylindrical condensor [energy width ΔE(FWHM) = 20–50 meV] [29, 35], a cylindrical mirror analyzer [ΔE(FWHM) = 6–35 meV] [19, 21, 23], and a two-stage hemispherical condensor [ΔE(FWHM) = 30–60 meV] [6, 15–18, 20, 22, 24–26]. The spectrometers were used with constant pass energy chosen to best meet the need of the actual experiment. The electrons, emitted from PI/AI processes in the reaction region, were imaged onto the entrance slit of the spectrometer by suitable electron optics. The energy-analyzed electrons were detected with a channel multiplier and fast counting electronics. Electron energy spectra were taken by multichannel scaling techniques. The resolution and energy-dependent transmission of the spectrometers were measured by HeI or NeI VUV photoelectron spectrometry of standard gases [39, 40], introduced to the reaction region through auxiliary gas inlets.

4 Results and discussion

4.1 He($2^3S, 2^1S$) + alkali, alkaline earth, Yb, and Hg atoms*

Discussion of the interaction of the metastable states of He with various atomic systems is an appropriate starting point because of their simplicity and amenability to accurate ab initio treatment [1, 6, 7, 15, 18, 21, 25, 41–46]. In addition, AI plays a much lesser role in these systems owing to the low polarizability of the ground state He atom and the correspondingly low attraction in the potential $V^+(R)$ of the ionic exit channel. The exception to this latter point is in the He*($2^3S, 2^1S$) + H systems (to be discussed below), for which the HeH^+ exit channel potential is strongly bound. Furthermore, the similarity in the valence electronic structure of

He*($1s2s\,^3$S) with that of Li($1s^2 2s\,^2$S) (in both instances the outer electron exhibits exchange repulsion from the region of the core electrons), suggests similar chemical interactions of these two atoms with a common target atom [1–4, 16, 41]; this trend will in fact be retrieved from the available data for potential well depths (see Table 2).

4.1.1 He*(2^3S, 2^1S) + alkaline earth, Yb, and Hg atoms

We start the discussion with the closed-shell target atoms Mg, Ca, Sr, Ba, Yb, and Hg. They all possess a closed outer ns^2 shell with ionization potentials for removal of one of the *ns* electrons ranging from 5.21 eV (Ba) to 10.44 eV (Hg). Production of the $A^+(ns\,^2S_{1/2})$ ground state is observed to be the preferred ionic exit channel [5, 15, 20, 47–50]. As a result of substantial electron correlation effects in the outer ns^2 shell, excited $A^+(np\,^2P_{1/2,3/2})$ ions are also formed with significant probability while other excited $A^+(nl)$ states may be also present, but with low probability [5, 15, 20, 47–50]. For Hg substantial ionization is also observed from the inner $5d^{10}$ shell [5, 47]. In contrast, ionization from the $4f^{14}$ shell of Yb atoms occurs with very low probability in collisions with He*(2^3S) atoms [20] even though 4*f* removal is prominent in the HeI (21.22 eV) and NeI (16.85 eV) VUV photoelectron spectra [51, 52]. This behavior represents a clear atomic example of the surface sensitivity of PI and reflects the fact that the radial density of the filled 4*f* shell is located rather close to the Yb nucleus while the density of the outer $6s^2$ electrons extends out much farther and thereby has a much greater overlap with the 1*s* hole in He* which has to be filled in the autoionization process [20]. The interaction in the entrance channel is best displayed in the electron spectra for the ionic ground state for which the He + $A^+(ns\,^2S_{1/2})\,^2\Sigma$ potential is only weakly attractive in the *R* range of interest and which is therefore well-suited for determination of the well depth D_e^* for the entrance channel curve $V^*(R)$. From calculations for, e.g., the system Li-Ca [53], one may expect the equilibrium internuclear distance in the entrance channel to lie around 6.7 a_0. Recent ab initio calculations for He* + Ca have yielded $R_e^* = 7.05\,a_0$ for He*(2^3S) + Ca and $R_e^* = 6.68\,a_0$ for He*(2^1S) + Ca [15].

The electron energy spectra resulting from PI processes occurring in thermal energy collisions of a mixed beam of He*(2^3S) and He*(2^1S) with ground state alkaline earth, Yb, and Hg atoms and leading to ground state ions $A^+(^2S_{1/2})$ are displayed in Fig. 4 on a common relative energy scale with the zero located at the respective nominal energy $^3E_0$ for the respective He*(2^3S) system [$^3E_0$ = excitation energy of He*(2^3S) minus the ionization energy of A forming ground state $A^+(ns\,^2S_{1/2})$]. Production of the ionic ground states $A^+(ns\,^2S_{1/2})$ by He*(2^1S) PI yields broader peak structure that is more substantially shifted to lower electron energies as compared with the He*(2^3S) produced peaks, in contrast with the alkali atom PI systems described below. Using the (resolution-corrected) low-energy "edge" values ε_m derived from analyses of the

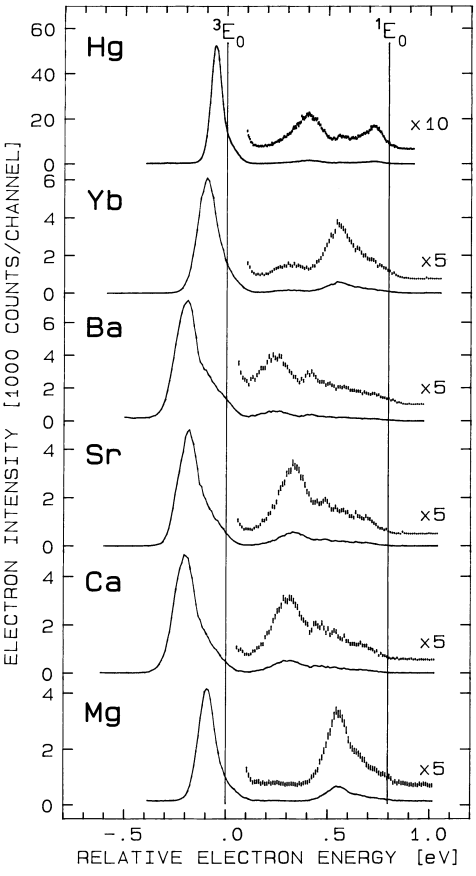

Fig. 4. Electron energy spectra resulting from ionizing collisions between He*(2^3S, 2^1S) atoms and the target atoms A = *Mg*, *Ca*, *Sr*, *Ba*, *Yb*, and *Hg* at average collision energies around 70 meV. The spectra are plotted on a common relative energy scale $\varepsilon - {}^3E_0$ [$^3E_0$ = excitation energy of He*(2^3S) minus the IP for formation of $A^+(ns\,^2S_{1/2})$]. The broad distributions between +0.1 eV and +1.0 eV are due to He*(2^1S) + A interactions, while the narrower distributions between −0.4 eV and +0.1 eV result from He*(2^3S) + A interactions. Note the complex peak structure in the He*(2^1S) + Yb, Hg electron spectra

$A^+(ns\,^2S_{1/2})$ peak structure shown in Fig. 4 and estimated values of $V_{ns}^+(R_e^*)$ of about zero for all the alkaline earth systems studied, we obtain values of the well depth D_e^* in the He*(2^3S) and He*(2^1S) entrance channels as given in Table 2. It is interesting to note that the ratios of the well depths for the He*(2^1S) + A systems and the He*(2^3S) + A systems, as determined for the alkaline earth atoms, are close to the respective ratios of the coefficients C_6 for the long-range van der Waals interaction [15]; the latter ratios mainly reflect the ratio of the polarizabilities for He*(2^1S) and He*(2^3S) (which amounts to 2.54). This is in contrast to the He* + alkali [16, 18, 44, 45] and especially the He* + H systems [6, 7, 17, 25, 41–43] where chemical bond formation and configuration interaction between the He*(2^3S) +A($^2\Sigma$) and the He*(2^1S) + A($^2\Sigma$) potential curves play an important role. The results for He*(2^3S) + Mg, Ca demonstrate similarity in the interactions with the respective Li-alkaline earth systems (calculated binding energies for LiMg and LiCa are 170 and 270 meV, respectively [53]).

Table 2. Experimentally evaluated well depths (D_e^*, in meV) for the lowest diatomic interaction potentials between Rg* and target atoms (A) from PI electron spectra (PIES) for the formation of the ground state ions A^+ (see text); for comparison some theoretical values and the well depths for Li($2\ ^2S$) + A have been included

	A = H	Li	Na	K	Rb	Cs	Mg	Ca	Sr	Ba	Yb	Hg
Li($2\ ^2S$)	2515[a]	1056[b]	876[b]	768[b]	720[b]	690[b]	170[c]	270[c]				105 (3)[d]
He*(2^3S)	2260 (45)[e]	868 (20)[f]	740 (25)[f]	591 (24)[f]	546 (18)[f]	533 (18)[f]	130 (25)[g]	250 (25)[g]	240 (25)[g]	260 (25)[g]	160 (20)[h]	90 (15)[i]
	2284[j]	855[k]	688[l]					243 (10)[m]				
He*(2^1S)	460 (50)[n]	330 (17)[f]	277 (24)[f]	202 (23)[f]	219 (18)[f]	277 (18)[f]	300 (25)[g]	570 (25)[g]	550 (25)[g]	670 (25)[g]	570 (40)[o]	490 (20)[i]
	426 (10)[p]	315[k]	250[l]					544 (15)[m]				
Ne*($^3P_2$)	2000 (100)[q]	798 (30)[r]	672 (20)[r]	561 (20)[r]								49 (7)[s]
	1890[t]		676 (18)[u]									
Ar*($^3P_2$)			602 (23)[u]									
Kr*($^3P_2$)			565 (26)[u]									
Xe*($^3P_2$)			555 (30)[u]									
Ne*($^3P_0$)	< 100[q]	35 (25)[r]	47 (18)[r]	30 (17)[r]								
			51 (19)[u]									
Ar*($^3P_0$)			107 (25)[u]									
Kr*($^3P_0$)			432 (30)[u]									
Xe*($^3P_0$)	1280 (200)[v]		530 (50)[u]									

[a] Predissociation spectroscopy Ref. [87]
[b] Spectroscopic results quoted in Ref. [16]
[c] Density functional calc. Ref. [53]
[d] Elastic scattering Ref. [88]
[e] PIES & calc. Ref. [70]
[f] Ref. [16]
[g] Ref. [15]
[h] Ref. [20]
[i] This work (assumed attraction in the exit channel $V^+(R_e^*) - V^+(\infty) \approx -5$ meV)
[j] Multireference configuration interaction (MRCI) calc. Ref. [7]
[k] MRCI calc. Ref. [26]
[l] MRCI calc. Ref. [18]
[m] MRCI calc. Ref. [15]
[n] Ref. [71]
[o] This work [assuming, in analogy to He* ($2\ ^1S$) + Ca [15], $V^+(R_e^*) - V^+(\infty) \approx 0$ meV]
[p] PIES & calc. Ref. [25]
[q] PIES & calc. Ref. [40]
[r] Ref. [29]
[s] Ref. [35]
[t] Ref. [60]
[u] Ref. [19]
[v] Diabatic model potential Ref. [37]

For Yb and Hg, the well depths for the $He^*(2^3S) + A$ systems are in line with the argument above that they reflect the long-range interaction. For $He^*(2^1S)$ + Yb, Hg, on the other hand, very interesting structured spectra are observed which point to the effects of interaction with other neutral channels. The $He^*(2^1S)$ + Hg spectrum was observed long ago [5, 47], but is not yet fully understood. The $He^*(2^1S)$ + Yb spectrum, reported here for the first time to our knowledge, has a width similar to that for $He^*(2^1S)$ + Hg, but differs in that the low energy peak has a smaller intensity than that for Hg. Candidates for perturbing neutral potential curves could be He + A** where A** denotes doubly excited states of Yb and Hg respectively. In view of the complexity of the $He^*(2^1S)$ + Yb, Hg spectra, we quote in Table 2 only the maximum well depths which have been derived from the respective lowest electron energy edges and reasonable estimates of final state interactions.

4.1.2 $He^*(2^1S, 2^3S)$ + alkali atoms

The electron energy spectra measured for collisions of a mixed He* beam with the alkali atoms Li, Na, K, Rb, and Cs are shown in Fig. 5 on a common relative energy scale whose zero-point corresponds to the respective nominal energy $^3E_0$ [16]. The broad distributions between +0.2 eV and −1 eV are due to the $He^*(2^3S)$ + A reactions proceeding through the $^2\Sigma$ interaction, while the narrower distributions between 1 eV and 0.4 eV are due to $He^*(2^1S) + A(^2\Sigma)$ reactions. The ratio of the $He^*(2^3S)/He^*(2^1S)$ flux was 6.9 in these measurements; thus the $He^*(2^1S)$ cross sections are 3–4 times larger than those for $He^*(2^3S)$ [16]. Autoionization out of the basically repulsive $^4\Sigma$ potential for the $He^*(2^3S)$ + A systems would lead to narrow (width < 100 meV) energy distributions located close to $^3E_0$. The absence of such a feature in all $He^*(2^3S)$ + alkali spectra clearly indicates that the quartet state is essentially inactive towards autoionization in accord with spin conservation in the Penning process.

All the spectra in Fig. 5 are characterized by peak structure dominantly residing below the nominal E_0 values, indicating attractive excited-state potentials $V^*(R)$ with well depths of the order of several tenths of an electron volt. The high-energy tail of the electron spectra ($\varepsilon > E_0$), representing the contribution to autoionization in the region $R \approx R_t^*$ (see Fig. 1), extends barely beyond E_0, as expected in view of the weak attraction in the He + A^+ potential. Correspondingly, AI processes ($\varepsilon \geq E_0 + E_{\rm rel}$) are negligible channels for both the $He^*(2^3S)$ + A and the $He^*(2^1S)$ + A systems. The low-energy "edges", $^{3,1}\varepsilon_m$ (see above), can be used in conjunction with estimates for the quantities R_e^* and $[V^+(\infty) - V^+(R_e^*)]$ as described in Ref. [16], to yield the well depth D_e^* in the $V^*(R)$ potential by Eq. (6). As can be seen from Table 2, the D_e^* values for the $He^*(2^3S) + A(^2\Sigma)$ interactions decrease monotonically from Li to Cs. These amount to about 80% of the well depths for the $Li(2s) + A(X\,^1\Sigma)$ systems [16]. The D_e^* values for the $He^*(2^1S) + A$ ($^2\Sigma$) interactions also decrease from Li to K, but then rise for Rb and Cs. This behavior may reflect the stronger influence of dispersive forces in the singlet He systems. Note that in a simple valence-bond description of the He* + A (A = alkali, H) systems the $He^*(2^3S)$ + A ($^2\Sigma$) potential curves are attractive (indicating formation of a chemical bond) while the $He^*(2^1S) + A(^2\Sigma)$ potentials are repulsive [41]. The substantial attraction of the latter systems reflects the effects of configuration interaction including the influence of the ionic $(He^+ + A^-)$ $^2\Sigma$ channel.

4.2 $Rg^*(^3P_2, ^3P_0)$ + alkali atoms

We have investigated two different aspects of Penning-type interactions between the heavier Rg atoms and alkali atoms. The first is the variation of A for the systems $Ne^*(3s\,^3P_2,^3P_0) + A$, (A = Li, Na, K), and the second is the variation of Rg* in the $Rg^*(ns\,^3P_2,^3P_0)$ + Na (Rg = Ne, Ar, Kr, Xe) systems. In the former, state-selected $Ne^*(3s\,^3P_2,^3P_0)$ beams were used to obtain the PI electron spectra of Li, Na, and K (yielding ground state alkali atoms) at thermal collision energies [29]. As also observed for $Ne^*(^3P_2,^3P_0) + H/D(1^2S_{1/2})$ [40], the spectra are very different for $Ne^*(^3P_2)$ and $Ne^*(^3P_0)$. In

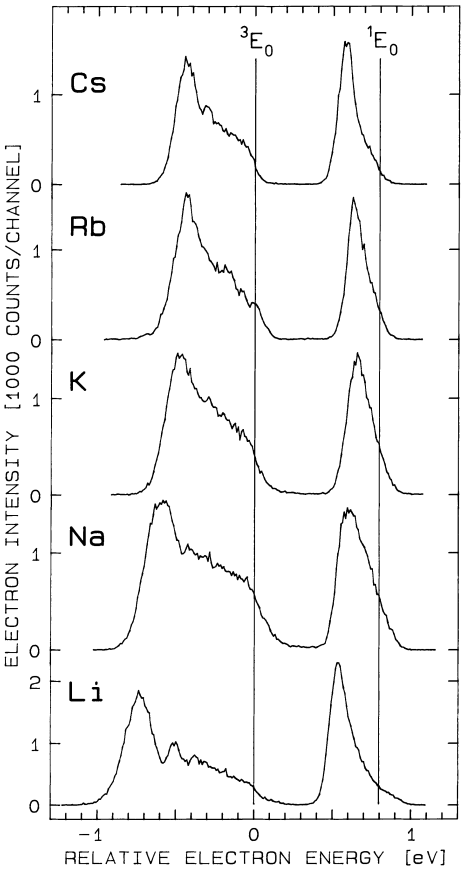

Fig. 5. Energy spectra of electrons released in thermal energy collisions of $He^*(2^3S)$ and $He^*(2^1S)$ with ground state alkali atoms A = *Li*, *Na*, *K*, *Rb*, and *Cs* on a common relative energy scale $\varepsilon - {}^3E_0$ [$^3E_0$ = excitation energy of $He^*(2^3S)$ minus the ionization potential of A]. The broad distributions between +0.2 eV and −1 eV are due to $He^*(2^3S) + A$, while the narrower distributions between 1 eV and 0.4 eV are due to $He^*(2^1S) + A$

the case of Ne*($^3P_2$), the spectra are very broad, and the main Airy-type peak structures are substantially shifted from their "nominal" energy positions $E_0(^3P_2)$. This is attributed to strongly attractive interaction potentials with well depths, $D_e^*(^3P_2) = 798(30)$ meV (Li), $= 672(20)$ meV (Na), $= 561(20)$ meV (K) (see Table 2). The equivalent peaks in the Ne*($^3P_0$) electron spectra are narrow and compatible with van der Waals-type attraction with well depths $D_e^*(^3P_0) < 50$ meV in all three target atomic systems [29].

In the other series of experiments we measured the electron energy spectra for the interaction of Rg*($ns\,^3P_2, ^3P_0$), (Rg = Ne, Ar, Kr, Xe), with ground state Na($3s\,^2S_{1/2}$) [19]. These spectra, corresponding to the formation of ground state Na^+ ions, are shown in Fig. 6 for the separate Rg components, Rg*($^3P_2$) and Rg*($^3P_0$), that are plotted on their respective common relative energy scale $\varepsilon - E_0$. As can be seen, the main peaks in the electron spectra due to Rg*($^3P_2$) + Na($3s$) collisions are universally shifted to large negative values of $\varepsilon - E_0$ (toward lower absolute electron energies), whereas only the Kr*($^3P_0$) and Xe*($^3P_0$) induced electron spectra are similarly shifted. This behavior reflects the strongly attractive nature of the entrance channel potential. In the case of the Ne*($^3P_0$) and Ar*($^3P_0$) + Na interactions, the peaks in the respective electron spectra are shifted from E_0 by a much lesser amount indicating weaker (van der Waals-type) entrance channel potentials. The physical reason for the differences between the Rg*($^3P_2$) + Na and the Rg *($^3P_0$) + Na interactions, as mirrored in the electron spectra, largely stems from the influence of spin-orbit splitting in the Rg* core which rises strongly from Ne* to Xe* [the $^3P_2 - ^3P_0$ energy separation increases from 0.096 eV (Ne*) to 1.132 eV (Xe*), see Table 1]. For Ne* + Na (and similarly for Ne* + H, Li, and K), the Ne*($^3P_0$) + Na ($\Omega = 1/2$) interaction potential lies close to several other $\Omega = 1/2$ potentials originating from the lower asymptotes Ne*($^3P_{2,1}$) + Na which prevent the former developing substantial attraction. In contrast, for Xe* + Na the Xe*($^3P_0$) + Na ($\Omega = 1/2$) potential is asymptotically located about 1 eV above the Xe*($^3P_{2,1}$) + Na ($\Omega = 1/2$) potentials, therefore exhibiting fewer interactions with the latter and correspondingly attaining a potential well of substantial depth which reflects chemical-type binding between the Xe*($6s$) electron and the Na($3s$) electron. Model calculations for the Rg*($^3P_2, ^3P_0$) + Na($3s\,^2S_{1/2}$) ($\Omega = 1/2$) interaction potentials by Morgner (see [19]), in which the exchange and the spin-orbit interactions in excited Rg and molecular interactions between the two valence s electrons (in terms of suitably chosen singlet and triplet potentials) are taken into account, nicely reflect the aspects discussed and the smooth transition in the observed behavior from Ne* to Xe*. It was found that autoionization in the Rg*($^3P_2$) + Na systems can be attributed predominantly to transitions from an attractive $^2\Sigma$ type quasi-molecule whose well depth is not far from that for the respective A(ns) + Na($3s$) ($^1\Sigma$) potential (A = Na, K, Rb, Cs, n = 3–6). For the Rg*($^3P_0$) + Na systems, on the other hand, van der Waals-type binding associated with basically quartet character was found for Rg* = Ne* (also explaining the low cross section for these systems) while a progressive admixture of the chemically bound configuration was observed from Ar* to Xe*. For Xe*, the especially strong effects of configuration mixing of the Xe*($6s\,^3P_0$) level with the close-by Xe*($5d, J = 0$) level (see, for example, Refs. [38, 54]) leads to a substantial admixture of the latter to the former. These effects were neglected in the model calculations, and it is quite likely that the special structure in the Xe*($^3P_0$) + Na($3s$) electron spectrum (see Fig. 6) is connected with the presence of molecular states originating from the Xe*($5d, J = 0$) +Na($3s$) asymptote. Led by the results of the model calculations for the entrance channel potentials $V^*(R)$ (regarding the choice of R_e^*) and using realistic ionic potentials $V^+(R)$, the well depths D_e^* for the relevant Rg* + Na potentials (see Table 2) were determined with a more elaborate procedure as described in Ref. [19].

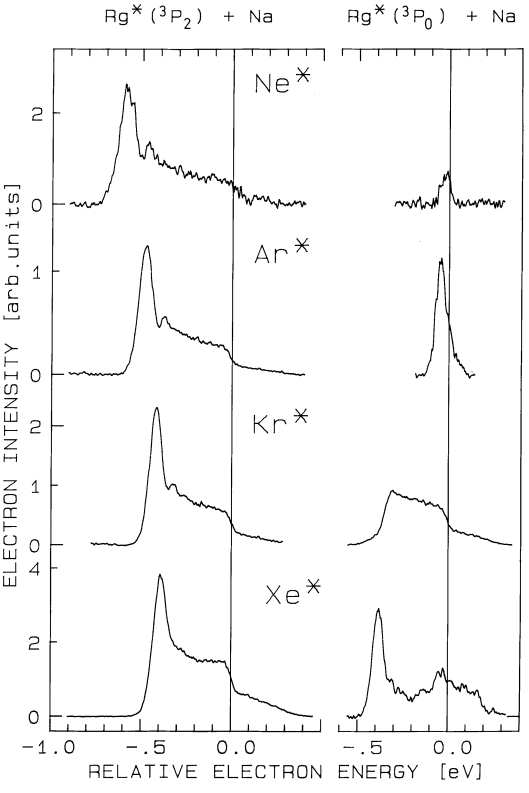

Fig. 6. Comparison of the electron energy spectra due to ionizing collisions of *Rg** (*ns* $^3P_2$), *Rg** (*ns* $^3P_0$) (Rg = Ne, Ar, Kr, Xe; n = 3, 4, 5, 6) with ground state Na($3s$) on a common relative energy scale $\varepsilon - E_0$, where E_0 = excitation energy of the respective *Rg** minus the ionization potential of *Na* (figure taken from Ref. [19]). For *Ne**, *Ar**, *Kr**, the two spectra are intensity-normalized such as to correspond to identical $^3P_2$ and $^3P_0$ fluxes. For *Xe**, the $^3P_0$ spectrum should be multiplied by a factor of about 4 in order to reflect a $^3P_2$:$^3P_0$ flux ratio of 60, as recently measured in Ref. [54], in contrast to the value of 15 obtained in Ref. [19] by extrapolation. The intensity scales for different Rg cannot be directly compared in terms of relative cross sections

4.3 Autoionization in collisions between Rg and H and determination of well depths for the $RgH^+(^1\Sigma)$ potentials (Rg = Ne, Ar, Kr, Xe)*

4.3.1 Associative PI and "true" AI in autoionizing Rg*-H collision complexes: a comparison

All Rg form strongly bound protonated molecular ions RgH^+ [55–59], and it is known that these ions can be produced in associatively ionizing thermal energy collisions of Rg* with ground state H [3]. Over the past few years numerous experimental and theoretical studies have addressed the dynamics of these autoionizing Rg-H collision complexes. In particular, detailed investigations of PI and AI were carried out on the basic collision system:

$$\mathrm{He}^*(2\,^3\mathrm{S}) + \mathrm{H}(1\,^2\mathrm{S})(^2\Sigma) \rightarrow \mathrm{He} + \mathrm{H}^+ + \mathrm{e}^-(\mathrm{PI}) \qquad (7a)$$

$$\rightarrow (\mathrm{He\text{-}H})^+ + \mathrm{e}^-(\mathrm{AI}) \ , \qquad (7b)$$

which may be regarded as a prototype system for autoionizing collision complexes at thermal energies. Combined theoretical and experimental studies have demonstrated that reactions (7a) and (7b) are very well described by local complex potential theory within the Born-Oppenheimer approximation [6, 7]. The entrance channel $V^*(R)$ is well-separated from the ionic curve $V^+(R)$ (i.e., electrons with energies of several eV are emitted) and other excited states are also quite distant. Therefore, the two-state potential curve model sketched in Fig. 1 provides an adequate description of the autoionization process in this model system. A somewhat more complicated, yet similar situation is met for the $\mathrm{Ne}^*(3s\,^3\mathrm{P}_2) + \mathrm{H}(1\,^2\mathrm{S})$ system [24, 40, 60] (see below). In both $\mathrm{He}^*(2\,^3\mathrm{S}) + \mathrm{H}$ and $\mathrm{Ne}^*(3s\,^3\mathrm{P}_2) + \mathrm{H}$ collisions, AI arises through autoionization near the classical turning point R_t^* in the entrance channel potential $V^*(R)$ with the ejected electron carrying away the excess energy. In contrast, for the heavier Rg^*,$\mathrm{Ar}^*(4s\,^3\mathrm{P}_2,^3\mathrm{P}_0)$, $\mathrm{Kr}^*(5s\,^3\mathrm{P}_2,^3\mathrm{P}_0)$, and $\mathrm{Xe}^*(6s\,^3\mathrm{P}_2,^3\mathrm{P}_0)$, where the excitation energy $E(\mathrm{Rg}^*)$ is lower than the ionization potential (IP) of the target $\mathrm{H}(1^2\mathrm{S})$, ionization can only occur by virtue of energy being gained through the formation of the $\mathrm{RgH}^+(^1\Sigma)$ diatomic bond between the collision partners upon ionization ("true" AI):

$$\mathrm{Rg}^* + \mathrm{H}(1^2\mathrm{S}) \rightarrow \mathrm{RgH}^+(v^+,J^+) + \mathrm{e}^-[\varepsilon(v^+,J^+)] \ . \qquad (8)$$

This situation is also met in other collision complexes with substantial ionic binding energy [14, 61, 62] such as metal-oxide systems. For both types of AI the energy $\varepsilon(v^+,J^+)$ for electrons associated with the formation of $\mathrm{RgH}^+(v^+,J^+)$ ions is simply given by:

$$\varepsilon(v^+,J^+) = E_0 + E_{\mathrm{rel}} + E_B(v^+,J^+) \ . \qquad (9)$$

Note that $E_0 = E(\mathrm{Rg}^*) - \mathrm{IP(H)}$ is negative for $\mathrm{Rg}^* = \mathrm{Ar}^*$, Kr^*, and Xe^*, while $E_B(v^+,J^+)$, the binding energy of the (v^+,J^+) state in the RgH^+ potential relative to the $\mathrm{Rg} + \mathrm{H}^+$ dissociation limit, is here defined to be positive.

In the case of the heavier Rg-H collision complexes two different mechanisms have been considered to explain the occurrence of "true" AI [4, 63]. The possible potential curves corresponding to these mechanisms are shown in Fig. 7. One proposed mechanism is characterized by heavy-particle motion along an adiabatic potential curve $V_a^*(R)$ that at all accessible distances of R lies below the ionic potential curve $V^+(R)$; therefore, $V_a^*(R)$ is real and ionization can only occur by dynamical coupling to the electronic continuum. An electron ejected in such an ionization process must gain its kinetic energy from the heavy-particle motion of the system, which is difficult to accomplish because the system attempts to remain in its instantaneous state. Hence, the associated electron spectrum is expected to have considerable intensity only close to zero electron energy in thermal collisions. The second mechanism can be described by evolution along a "diabatic" potential curve $V_d^*(R)$ which crosses into the $\mathrm{RgH}^+ + \mathrm{e}^-$ continuum at some internuclear distance R_C. Toward small distances the potential $V_d^*(R)$ acquires an imaginary part $-i\Gamma(R)/2$, so for $R \leq R_C$ the system may decay into the $\mathrm{RgH}^+ + \mathrm{e}^-$ continuum by an electronic transition of local rate $\Gamma(R)/\hbar$, as in the case of PI/AI (we note that the width $\Gamma(R)$ extends to distances $R > R_C$ reflecting loss processes into the dense $(\mathrm{RgH})^{**}$ Rydberg manifold associated with the RgH^+ potential [64]). It should, therefore, be possible to apply, with appropriate modifications, the standard theory of PI/AI (developed for situations as in Fig. 1) to "true" associative autoionization from the diabatic path. In contrast to the dynamical coupling mechanism, the energy of ejected electrons is not limited to small values. Hence, in prin-

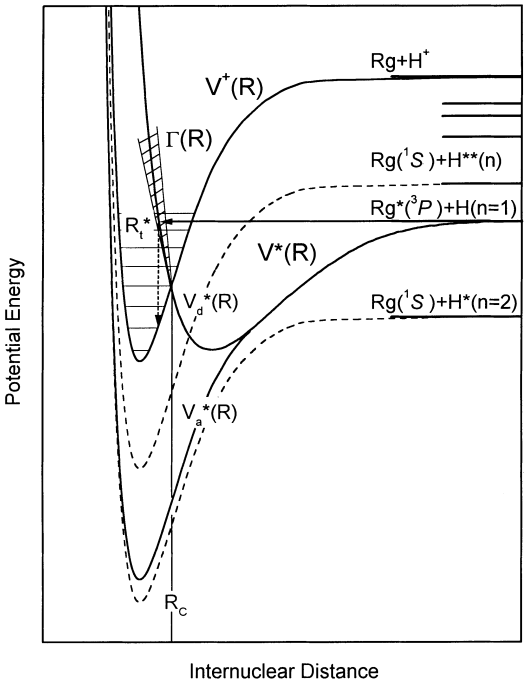

Fig. 7. Schematic representation of the possible potential energy curves involved in "true" associative PI for *Rg*-H* collision complexes in which the asymptotic energy of the incoming channel $V^*(R)$ for the Rg* (^3P_J) + $H(1s)$ collision system lies below the asymptotic energy of the associative ion potential $V^+(R)$. For an explanation of the other potential curves presented see text

ciple, the energy characteristics of the electron spectra may be used to distinguish between the two mechanisms.

From Eq. (9) it is clear that for a particular, well-defined collision energy, the energy spectrum $P(\varepsilon)$ of electrons ejected in reaction (8) yields direct information on the final vibrational-rotational state distribution of the associated molecular ions $RgH^+(v^+,J^+)$. Therefore, a measurement of $P(\varepsilon)$ with high-energy resolution can provide detailed information on the potential energy curve for RgH^+, as well as on the entrance channel potential energy curve, through accurate evaluation of the observed energy levels and determination of the (v^+,J^+) distribution. From an experimental point of view, AI in reactions (7b) and (8) is a favorable case for such studies because the molecular ions RgH^+, in general, possess large vibrational frequencies and rotational constants [55–59, 65–68]. In real electron spectrometric experiments, however, each of the discrete peaks involved in Eq. (9) is broadened by the influence of the distribution of collision energies E_{rel} and by the finite energy resolution of the spectrometer. In the experiments described here, the rich vibrational-rotational structure in the AI electron spectra is therefore partially obscured by the thermal collision energy distribution ($T \approx 300$ K) that was used (for intensity reasons) and by the bandwidth of the electron spectrometer (about 35 meV).

Figure 8 shows a comparison between the experimental electron energy distributions due to autoionizing collisions of ground-state atomic H with $He^*(2^3S_1)$ [6, 22], $Ne^*(3s\,^3P_{2,0})$ [24], and $Ar^*(4s\,^3P_{2,0})$ [69] atoms

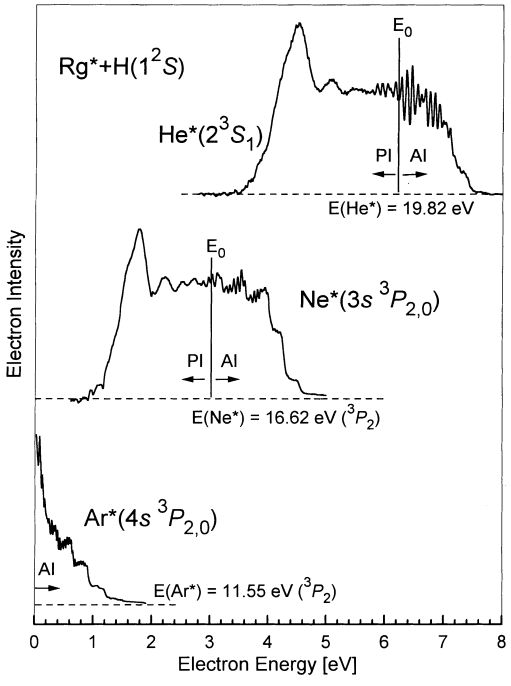

Fig. 8. Comparison of electron energy spectra derived from the $Rg^* + H(1^2S)$ collision systems ($Rg^* = He^*(2^3S_1)$, Ne^* $(3s^3P_{2,0})$, $Ar^*(4s^3P_{2,0})$) showing the contributions to the spectra due to PI and AI. E_0 is the "nominal" energy = excitation energy of Rg^* minus the IP of the H

at thermal kinetic energies ($\langle E_{rel}\rangle \approx 0.05$ eV). All spectra were measured in a crossed beams configuration at the fixed detection angle $\Theta = 90°$ with respect to the average collision velocity vector of the collision system. The energy spectrum of electrons for the system $He^*(2^3S) + H(1^2S)$ shown in the upper trace of Fig. 8 displays a very broad distribution and an Airy-type interference pattern at energies $\varepsilon \leq 5.8$ eV that is associated with two coalescent points of stationary phase due to a well-characterized minimum in the energy function $\varepsilon(R) = V^*(R) - V^+(R)$. Furthermore, distinct structure due to the formation of quasi-bound rovibrational levels of $HeH^+(v^+,J^+)$ with high J^+ values of around 25 in the range $5.8 \leq \varepsilon \leq 6.27$ eV is observed. In addition, partially resolved rovibronic structure due to the formation of truly bound $HeH^+(v^+,J^+)$ levels is observed at electron energies $\varepsilon > 6.27$ eV, i.e., at $\varepsilon > E_0 + \langle E_{rel}\rangle$, where E_0 is as defined above. The contribution of AI to the full spectrum amounts to 23% for the $He^*(2^3S) + H(1^2S)$ collision complex [6, 22]. Similar behavior has been observed for the electron spectrum resulting from $Ne^*(3s\,^3P_2) + H(1^2S)$ autoionizing collisions [24, 40, 69]. This spectrum is also very broad and again shows a clear Airy-type interference structure (energies $\varepsilon \leq 2.8$ eV). It contains a substantial fraction of about 30% due to AI at electron energies $\varepsilon > 3.07$ eV, where the partially resolved rovibronic structure indicates the formation of bound molecular ions $NeH^+(v^+,J^+)$. This type of structure continues into the PI regime of the spectrum down to $\varepsilon \cong 2.8$ eV, as a result of the formation of quasi-bound rovibrational levels. In contrast, the spectrum for $Ne^*(^3P_0) + H(1^2S)$ consists of a sharp peak close to E_0 [40], reflecting – as observed for $Ne^*(^3P_0) + A(ns\,^2S)$ (A = Li, Na, K) [29], see above – weak, van der Waals-type attraction. The corresponding ionization cross section is almost two orders of magnitude smaller than the one for $Ne^*(^3P_2) + H(1^2S)$ collisions; therefore the $^3P_0$ contribution to the mixed $Ne^*(^3P_{2,0}) + H(1^2S)$ spectrum shown in Fig. 8 is negligible.

For the systems $Ar^*(4s\,^3P_{2,0}) + H(1^2S)$, the $(Ar + H^+)$ potential is asymptotically about 2 eV higher than the entrance channel potential, therefore PI cannot occur. "True" AI (Eq. 8) is possible, however, if the classical turning point in the entrance channel potential is located within the strongly attractive ArH^+ potential, and AI does indeed occur with a cross section close to $10^{-20}\,m^2$ for both $Ar^*(^3P_2)$ and $Ar^*(^3P_0)$ [37]. The similarity of the general shape of the Ar* induced AI electron spectrum with the AI part of the $He^*(2^3S) + H$ and $Ne^*(^3P_2) + H$ spectra (see Fig. 8) indicates that electron emission occurs through electronic autoionization from a diabatic potential curve of $Ar^* + H$ into the $ArH^+ + e^-$ continuum (the mixed $Ar^* + H$ spectrum is predominantly due to $Ar^*(^3P_2)$ because of its higher flux, see Table 1). Through recent systematic mass spectrometric as well as electron spectrometric investigations of AI in the systems $Rg^*(ns\,^3P_2,^3P_0) + H(1^2S)$, $D(1^2S)$ (Rg = Ar, Kr, Xe) (n = 4, 5, 6), which included Rg^* state selection by diode lasers (see Sect. 3), it was possible to determine the absolute AI cross sections for these 12 collision pairs and – with the help of quantum mechanical model calculations for the electron spectra –

to draw detailed conclusions on the autoionization mechanism involved [37] (see also the discussion below). Here we concentrate on the aspect of how accurate RgH^+ potential well depths were determined from the AI electron spectra for the respective Rg* + H collision complexes.

4.3.2 Structural information on the Rg* + H potential curves and well depths for the RgH^+ systems (Rg = Ne, Ar, Kr, Xe) from analyses of the AI electron spectra

A detailed ab initio treatment of the autoionization process in the basic molecular collision complex $He^*(2^3S) + H(1^2S)$ was recently carried out by Movre and Meyer [6, 7]. The well depth of the relevant $He^*(2^3S) + H(^2\Sigma^+)$ entrance channel potential curve, $D_e^* = 2.284$ eV, agrees very well with the experimental value, $D_e^* = 2.260(45)$ eV, determined by Morgner and Niehaus [70] from their PI electron spectra and also with the first experimental estimate of $D_e^* = 2.44(20)$ eV [71]. For the $He^*(2^1S) + H(^2\Sigma^+)$ potential Movre and Meyer calculated a well depth of $D_e^* = 0.426$ eV [7, 25], which is in agreement with the first PI electron spectrometric result $D_e^* = 0.46(5)$ eV [71]. Comparisons of the measured angular dependent electron spectra for both $He^*(2^3S) + H(^2\Sigma)$ [6, 7] and $He^*(2^1S) + H(^2\Sigma)$ [25] with the quantum mechanical results [6, 7, 25] indicate that the calculated well depths for these systems are accurate to within 20 meV or better. Ab initio studies of the Rg* + H systems involving the heavier Rg atoms are scarce due to their increased complexity associated with the spin orbit split Rg ion core and because of their mixing – for Rg = Ar, Kr, and Xe – with the nearby $Rg + H^*(n \geq 2)$ Rydberg channels. Ab initio calculations of the adiabatic $^2\Sigma$ and $^2\Pi$ potential curves for the heavier $(Rg\text{-}H)^*$ systems [72–75] were carried out in LS-coupling for the Rg* atoms [ignoring the fine-structure in $Rg^*(^3P)$] and therefore cannot be directly used in model calculations of PI/AI processes.

Through quantum mechanical model studies of PI and AI in $Ne^*(3s\,^3P_2) + H(1^2S)$ collisions Lorenzen et al. [40] and Khan et al. [60] extracted information on the complex entrance channel potential by fitting the electron energy spectrum [40] and by fitting both the electron and the ion angle-energy distributions [60]. Both studies came to the conclusion that a single optical potential, corresponding to an autoionizing state of Ne* + H with $^2\Sigma^+$ symmetry, consistently represents the main features of the experimental data. Khan et al. have chosen the spectroscopic RKR potential for NaH ($X\,^1\Sigma^+$) ($D_e^* = 1.975$ eV [76]) as a starting point for the fitting procedure of the real part of the complex entrance channel potential and evaluated a well depth of $D_e^*[Ne^*(^3P_2) + H] = 1.89$ eV [60] while Lorenzen et al. [40] obtained a well depth of $D_e^* = 2.0(1)$ eV. On the basis of additional theoretical analyses and experimental spectra for the $Ne^*(3s\,^3P_2) + H(1\,^2S)$ system, Merz et al. [24] proposed using a potential $V^*(R)$ which includes that of Khan et al. at large internuclear distances down to the well region and joins the potential of Lorenzen et al. (which yields a good description of the low v^+ AI spectrum) at shorter range.

Experimental well depths D_e^+ of the ionic potential curves $V^+(R)$ for NeH^+ and ArH^+ have been derived by Lorenzen et al. [69] to within ±32 meV through analyses of the high-energy AI part of the electron spectra in $Ne^*(3s\,^3P_2) + H(1^2S)$ and $Ar^*(4s\,^3P_{0,2}) + H(1^2S)$ colli-

Table 3. Structural properties and binding energies of $RgH^+(^1\Sigma^+)$ ions (all well depths D_e^+ refer to the dissociation limit with the lowest energy; energy conversion: 1 eV = 8065.541 cm^{-1})

		$^{20}NeH^+$	$^{40}ArH^+$	$^{84}KrH^+$	$^{132}XeH^+$
r_e (10^{-10} m)	(theory)	0.996 (3)[a]	1.286 (3)[b]	1.419 (3)[a]	1.611 (5)[c]
	(exp.)	0.9912[d]	1.2804[e]	1.4212[e]	1.6028[f]
ω_e (cm^{-1})	(theory)	2896 (20)[a]	2723 (20)[b]	2561 (20)[a]	2313 (50)[c]
	(exp.)	2903.75[d]	2710.92[e]	2494.65[e]	2269.97[f]
$\omega_e x_e$ (cm^{-1})	(theory)	113[a]	56[b]	49[a]	41 (5)[c]
	(exp.)	113.36[d]	61.64[e]	48.53[e]	41.32[f]
D_e^+(eV)	(theory)	2.280 (50)[a]	4.057 (50)[b]	4.807 (50)[a]	4.04 (10)[c]
	(exp.)	2.275 (25)[g]	4.025 (30)[g]	4.805 (30)[g]	4.00 (3)[g]
		2.28 (10)[h]	4.04 (10)[i]	4.45 (10)[h]	5.28[h]
		2.27[j]	4.22[j]	4.6[j]	
			4.17[k]		
		2.300[l]	4.147[l]		

[a] Ref. [57]. Results of ab initio coupled electron-pair approximatic (CEPA) calculations
[b] Ref. [56]. Results of ab initio CEPA calculations
[c] Ref. [58]. Results of ab initio CEPA calculations
[d] Ref. [67]. Spectroscopic results
[e] Ref. [66]. Spectroscopic results
[f] Ref. [68]. Spectroscopic results
[g] Present work, AI electron spectrometry. Values determined by analysis of experimental data in Refs. [24, 37, 69]. We note that the vibrational quantum numbers in Fig. 3 of Ref. [24] are incorrect and have to be raised by one unit. D_e^+ value for XeH^+ corresponds to a proton affinity of Xe of 5.474 (30) eV
[h] Ref. [79] Values derived from analysis of elastic H^+ + Rg scattering; result for XeH^+ calculated from the quoted value for the proton affinity of 6.75 eV
[i] Ref. [78]. Value derived from analysis of elastic H^+ + Rg scattering
[j] Ref. [77]. Value derived from analysis of elastic H^+ + Rg scattering
[k] Ref. [80]. Value derived from analysis of elastic H^+ + Rg scattering
[l] Ref. [81]. Value derived from analysis of elastic H^+ + Rg scattering

sion systems leading to the associated molecular ions $NeH^+(v^+,J^+)$ and $ArH^+(v^+,J^+)$, respectively. Fit calculations were carried out to approximate the shape of the onset observed for low-lying vibrational levels v^+ of the molecular ions RgH^+ with the aim to extract the energy position of the respective rotationless vibrational $RgH^+(X\,^1\Sigma^+, v^+, J^+ = 0)$ levels. By fitting these energy values to the formula

$$E_B(v^+, J^+ = 0) = D_e^+ - \omega_e(v^+ + 1/2) + \omega_e x_e(v^+ + 1/2)^2 \tag{10}$$

the energy value for the $v^+ = 0$ level and the well depth D_e^+ of the ionic system were obtained [69] and good agreement with the results of coupled electron-pair approximation (CEPA) ab initio calculations (estimated uncertainty ± 50 meV) [56, 57] was found (see Table 3). As mentioned above, electron energy spectra from AI in thermal energy collisions of state-selected heavier Rg* (Rg = Ar, Kr, Xe) with H have only recently become available [37]. Electron spectrometry reveals that at electron energies above about 0.2 eV the shape of the AI spectra from reaction (8) is similar to the high energy, AI part of the electron energy distributions for the collision systems $He^*(2^3S) + H(1^2S)$ and $Ne^*(3s\,^3P_2) + H(1^2S)$ (see Fig. 8). Quantum mechanical model calculations of the electron spectra for reaction (8) indicate that the AI processes associated with electron energies $\varepsilon \geq 0.2$ eV can be well described by electronic decay from a (diabatic) local complex potential $V_d^*(R) - i\Gamma(R)/2$ with suitably chosen real and imaginary parts. It turns out that the most critical parameters are the crossing point R_C of $V_d^*(R)$ with the ionic potential $V^+(R)$ for RgH^+ and the slope of $V_d^*(R)$ around R_C (see Fig. 8), as was demonstrated in detail [37] for the relatively simple model system $Xe^*(6s\,^3P_0) + H(1^2S)$ for which the density of other nearby excited (Rg-H)* states is rather low (at least at large and intermediate internuclear distances). Figure 9 shows a comparison between the experimental electron energy spectrum and quantum mechanical model calculations for AI in thermal $Xe^*(6s\,^3P_0) + H(1^2S)$ collisions. Good overall agreement between theoretical and experimental results is observed at energies above about 0.2 eV. The model fails to reflect, however, the significant increase of electron intensity toward $\varepsilon = 0$ eV that occurs in each experimental spectrum of the heavier Rg-H complexes [37]. This deviation demonstrates limitations of the simple diabatic model based on the local complex potential approximation and possibly indicates contributions from a dynamical coupling mechanism. A detailed discussion of the model used to describe AI in the heavier Rg-H systems will be given in a future paper.

In the lower part of Fig. 9, we show the calculated separate vibrational contributions to the $Xe^*(6s\,^3P_0) + H(1^2S)$ AI electron energy spectrum. They reveal that the step-like increases of electron intensity in the full spectrum are (predominantly) due to the access of particular v^+ vibrational levels at low J^+ values in the exit channel. To aid in identifying the onset of the various (v^+, J^+) state contributions to the overall electron spectrum we have indicated the energy location of the $J^+ = 0$

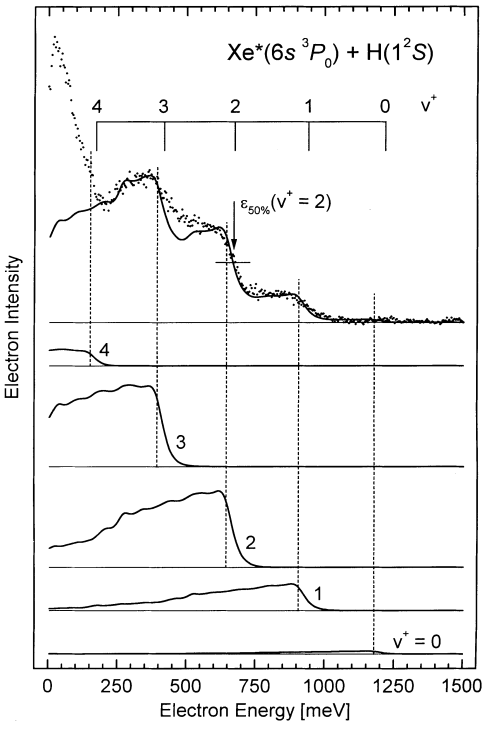

Fig. 9. Comparison between the experimental electron energy spectrum (*dots*) and quantum mechanical model calculations (*solid lines*) for "true" AI in the thermal energy $Xe^*(6s\,^3P_0) + H(1^2S)$ collision system, showing the contributions of final-state vibrational populations v^+ to the overall electron spectrum. The vertical *dashed lines* indicate the energy location of the $J^+ = 0$ state within the respective vibrational level for the case of zero collision energy, as obtained in our model fit calculation; the *vibrational grid* in the *upper part* of the figure denotes the respective energy positions as obtained from the ab initio calculation [58]. See text for a discussion of the substantial difference between the calculated and the measured electron spectrum at energies below about 0.2 eV

state within each vibrational level for the case of zero collision energy, both for the ab initio calculation [58] and for our model fit calculation. Comparison between the measured and the calculated AI electron spectra (the RgH^+ well depth is treated as an adjustable parameter within the estimated uncertainty interval of the ab initio well depth [58]) yields an unambiguous vibrational assignment. Furthermore, a simple and useful criterion for determination of the rotationless binding energies $E_B(v^+, J^+ = 0)$ can be established from the 50% intensity point $\varepsilon_{50}(v^+)$ of the step-like increase of the vibrational onset:

$$E_B(v^+, J^+ = 0) = \varepsilon_{50}(v^+) - \{E_{\mathrm{rel}}\} + \mathrm{IP(H)} - E(\mathrm{Rg}^*)\ , \tag{11}$$

where $\{E_{\mathrm{rel}}\}$ denotes an effective collision energy which corresponds to the 50% intensity point of the vibrational onset (see Fig. 9). From the calculations for $Xe^*(6s\,^3P_0) + H(1^2S)$ shown in Fig. 9 (which represent the proper average over the experimental collision energy distribution, average collision energy $\langle E_{\mathrm{rel}} \rangle = 50$ meV) we find the value $\{E_{\mathrm{rel}}\} = 25$ meV. We have also used this value for evaluation of the binding energies $E_B(v^+, J^+ = 0)$ for step-like vibrational

onsets in the electron spectra of the other Rg* + H systems. Since the rovibrational energies in the RgH^+ potentials are well-known from infrared spectroscopy [65–68] (at least at low v^+) it is sufficient, for accurate determination of the dissociation energy, D_0, and for the well depth, D_e^+, to extract the binding energy $E_B(v^+, J^+ = 0)$ of just one v^+ level from the AI electron spectrum as long as the vibrational numbering is certain.

Table 3 summarizes the values for the well depths D_e^+ of the $RgH^+(^1\Sigma)$ ions, as evaluated from the experimental vibrational onset energies $\varepsilon_{50}(v^+)$ in conjunction with Eqs. (10) and (11), referred to the respectively lowest dissociation asymptote (in all cases except for XeH^+, the $Rg + H^+$ asymptote is the lowest); the spectroscopic values [65–68] for ω_e and $\omega_e x_e$ were used in Eq. (10). The corresponding proton affinities of the Rg atoms (including HeH^+ with $D_e^+ = 2.040$ [55]) fall in the range 2.04 to 5.47 eV and rise toward heavier Rg. It is interesting to note that the quantity $\alpha/(2R_e^{+4})$ (which is a measure of the polarization attraction at the equilibrium distance) is constant (within 1%) for ArH^+, KrH^+, and XeH^+. The well depths for NeH^+, ArH^+, KrH^+, and XeH^+, calculated by the CEPA method [56–58], are in all cases in excellent agreement with the values derived from the AI electron spectra. For NeH^+, the well depths extracted from analyses of H^+-Rg scattering experiments [77, 79, 81] agree with our result, whereas for ArH^+ they are too high [77, 80, 81] with one exception [78]. In particular, the well depth of 4.147 eV, determined by Gianturco et al. [81, 82] through a multiproperty analysis, is not compatible with our AI electron spectrometric result of 4.025(30) eV (see also the discussion in Ref. [59]). For the systems $Kr + H^+$ [77, 79, 83] and $Xe + H^+$ [79, 83], differential scattering cross sections have also been reported, but the multichannel nature of the problem complicates the analysis, and, to our knowledge, no accurate well depths for KrH^+ and XeH^+ have been determined from scattering experiments so far.

5 Conclusions

High-resolution electron spectrometry of autoionizing diatomic complexes (Rg-A)*, formed in thermal energy collisions between Rg* and A, provides a powerful tool to derive detailed structural information on the RgA* quasi-molecule (in particular its binding energy) and – in cases of substantial attraction in the final ionic state – also on the RgA^+ pair. In this paper we have summarized our present knowledge on the interaction potentials of Rg* with H alkali, alkaline earth, Yb, and Hg atoms including well depths for the RgH^+ ions. Except for a few systems with pure long-range attraction such as $Ne^*(^3P_0)$ + H, Li, Na, K (well depths < 50 meV [19, 29, 40]) and for the special case $He^*(2^3S) + H(1^2S)$ ($D_e^* = 2.284$ eV [7]) these quasimolecules are characterized by well depths in the range 0.1 to 1 eV. The potential of electron spectrometry for rather accurate determination of the well depths, $D_e^* = V^*(R_e^*)$, stems from the fact that electron emission from the region around the well is associated with a clear Airy-type peak in the electron spectrum, $P(\varepsilon)$, whose shape is (almost) independent of the collisional impact parameter and whose low-energy edge provides an experimental value for the well depth in a rather direct and simple way. Note that optical spectroscopy, which is the standard method for the determination of well depths for ground state systems, does in general not work for autoionizing collision complexes because photon emission is improbable (except for cold collisions [84]). Elastic scattering studies have provided detailed information for weakly bound ionizing collision systems such as He* + Ar through the analysis of rainbow and glory scattering [1, 85]. For systems with well depths D_e^* larger than the collision energy, however, orbiting occurs; the resulting differential scattering cross sections are very complex and extraction of accurate well depths from analysis of the experimental data is problematic (see, for example, Ref. [86]). Elastic scattering experiments with heated or seeded supersonic beams, which could provide collision energies sufficiently high to observe rainbow scattering, may yield independent structural information on many of the systems which we have reported in this paper.

Acknowledgements. This work was supported by the Deutsche Forschungsgemeinschaft (DFG) through Ho 427/19 and Forschergruppe "Schwellenverhalten, Resonanzen und nicht-lokale Wechselwirkungen bei niederenergetischen Elektronenstreuprozessen". Financial support for T.E.R from the Graduiertenkolleg "Laser und Teilchenspektroskopie" is gratefully acknowledged. A.J.Y acknowledges financial support from the DFG and hospitality at the Fachbereich Physik of the Universität Kaiserslautern. Over the past few years, our work on PI and AI electron spectrometry involving excited atoms has had many contributors to whom we are indebted and grateful; in particular, we thank T. Bregel, W. Bussert, H. Dengel, J. Lorenzen, H.A.J. Meijer, A. Merz, H. Morgner, M. Movre, M.W. Müller, S. Schohl, and H. Waibel. Finally, special acknowledgement and thanks go to Wilfried Meyer whose interest, effort and theoretical insight into the dynamics of autoionizing collision complexes fostered our better understanding of experimental electron energy spectra of Penning-type systems.

References

1. Siska PE (1993) Rev Mod Phys 65:337
2. Yencha AJ (1984) In: Brundle CR, Baker AD (eds) Electron spectroscopy, theory, techniques and applications, vol 5. Academic Press, New York, p 197
3. Niehaus A (1981) Adv Chem Phys 45:399
4. Hotop H (1980) In: Oda N, Takayanagi K (eds) Electronic and atomic collisions. North Holland, Amsterdam, p 271
5. Hotop H, Niehaus A (1969) Z Phys 228:68
6. Merz A, Ruf M-W, Hotop H, Movre M, Meyer W (1994) J Phys B 27:4973
7. Movre M, Meyer W (1997) J Chem Phys 106:7139
8. Nakamura H (1969) J Phys Soc Jpn 26:1473
9. Miller WH (1970) J Chem Phys 52:3563
10. Morgner H (1990) Chem Phys 145:239
11. Cermak, V, Ozenne JB (1971) Int J Mass Spectrom Ion Phys 7:399
12. Longley EJ, Dunlavy DC, Falcetta MF, Bevsek HM, Siska PE (1993) J Phys Chem 97:2097
13. Ohno K, Yamakado H, Ogawa T, Yamata T (1996) J Chem Phys 105:7536
14. Dyke JM, Shaw AM, Veszpremi T (1997) J Chem Soc Faraday Trans 93: 2631

15. Ruf M-W, Yencha AJ, Hotop H, Movre M, Kerner C, Zillig S, Meyer W (1996) Z Phys D 37:219
16. Ruf M-W, Yencha AJ, Hotop H (1987) Z Phys D 5:9
17. Waibel H, Ruf M-W, Hotop H (1988) Z Phys D 9:191
18. Merz A, Müller MW, Ruf M-W, Hotop H, Meyer W, Movre M (1990) Chem Phys 145:219
19. Schohl S, Müller MW, Meijer HAJ, Ruf M-W, Hotop, Morgner H (1990) Z Phys D 16:237
20. Hotop H, Ruf M-W, Yencha AJ, Fricke B (1990) Ann Phys (Leipzig) 47: 625
21. Müller MW, Merz A, Ruf M-W, Hotop H, Meyer W, Movre M (1991) Z Phys D 21:89
22. Merz A, Ruf M-W, Hotop H (1992) Phys Rev Lett 69:3467
23. Dengel H, Ruf M-W, Hotop H (1993) Europhys Lett 23:567
24. Merz A, Ruf M-W, Hotop H (1994) Z Phys D 32:197
25. Movre M, Meyer W, Merz A, Ruf M-W, Hotop H (1994) Chem Phys Lett 230:276
26. Merz A, Müller MW, Ruf M-W, Hotop H, Meyer W, Movre M (1989) Chem Phys Lett 160:377
27. Hotop H, Niehaus A (1970) Z Phys 238:452
28. Gerber G, Niehaus A (1976) J Phys B 9:123
29. Lorenzen J, Hotop H, Ruf M-W (1986) Z Phys D 1:261
30. Bieniek RJ, Müller MW, Movre M (1990) J Phys B 23:4521
31. Weber JM, Hansen K, Ruf M-W, Hotop H (1998) Chem Phys (in press)
32. Hotop H (1996) In: Dunning FB, Hulet RG (eds) Experimental methods in the physical sciences, vol. 29B Academic Press, San Diego, p 191
33. Hotop H, Niehaus A, Schmeltekopf AL (1969) Z Phys 229:1
34. Dunning FB, Cook T, West WP, Stebbings RF (1975) Rev Sci Instrum 46: 1072
35. Hotop H, Lorenzen J, Zastrow A (1981) J Electron Spectrosc Relat Phenom 23:347
36. Weissmann G, Ganz J, Siegel A, Waibel H, Hotop H (1984) Opt Common 49:335
37. Roth T (1998) Dissertation. Universität Kaiserslautern Shaker Verlag, Aachen, ISBN 3-8265-4290-8
38. Kau R, Petrov ID, Sukhorukov VL, Hotop H (1998) J Phys B 31:1011
39. Samson JAR, Gardner JL (1976) J Electron Spectrosc Relat Phenom 8:469
40. Lorenzen J, Morgner H, Bussert W, Ruf M-W, Hotop H (1983) Z Phys A 310:141
41. Miller WH, Schaefer III HF (1970) J Chem Phys 53:1421
42. Miller WH, Slocomb CA, Schaefer HF III (1972) J Chem Phys 56:1347
43. Hickman AP, Isaacson AD, Miller WH (1977) J Chem Phys 66:1483
44. Cohen JS, Martin RL, Lane NF (1985) Phys Rev A 31:152
45. Padial NT, Cohen JS, Martin RL, Lane NF (1989) Phys Rev A 40:117
46. Sarpal BK (1993) J Phys B 26:4145
47. Cermak V, Herman Z (1968) Chem Phys Lett 2:359
48. Gerard K, Hotop H, Mahr D (1977) Adv Mass Spectrom 7A:192
49. Inaba S, Goto T, Hattori S (1981) J Phys B 14:507
50. Inaba S, Goto T, Hattori S (1983) J Phys Soc Jpn 52:1164
51. Lee ST, Süzer S, Matthias E, Rosenberg RA, Shirley DA (1977) J Chem Phys 66:2496
52. Kerling C, Böwering N, Heinzmann U (1989) Abstracts Contrib Papers XVI. ICPEAC, New York, p 9, and private communication
53. Jones RO (1980) J Chem Phys 72:3197
54. (a) Kau R, Petrov ID, Sukhorukov VL, Hotop H (1997) Z Phys D 39:267; (b) Kau R, Petrov ID, Sukhorukov VL, Hotop H (1997) Z Phys D 42:318
55. Kolos W, Peek JM (1976) Chem Phys 12:381
56. Rosmus P (1979) Theor Chim Acta 51:359
57. Rosmus P, Reinsch E-A (1980) Z Naturforsch Teil A 35:1066
58. Klein R, Rosmus P (1984) Z Naturforsch Teil A 39:349
59. Hirst DM, Guest MF, Rendell AP (1992) Mol Phys 77:279
60. Khan A, Siddiqui HR, Siska PE (1991) J Chem Phys 94:2588
61. Weiner J, Masnou-Seeuws F, Giusti-Suzor A (1990) Adv At Mol Opt Phys 26:209
62. Klucharev AN (1993) Physics-Uspekhi 36:486
63. Nakamura H (1971) J Phys Soc Japan 31:574
64. Miller WH, Morgner H (1977) J Chem Phys 67:4923
65. Brault JW, Davis SP (1982) Phys Scr 25:268
66. Johns JWC (1984) J Mol Spectrosc 106:124
67. Ram RS, Bernath PF, Brault JW (1985) J Mol Spectrosc 113:451
68. Rogers SA, Brazier CR, Bernath PF (1987) J Chem Phys 87:159
69. Lorenzen J, Hotop H, Ruf M-W, Morgner H (1980) Z Phys A 297:19
70. Morgner H, Niehaus A (1979) J Phys B 12:1805
71. Hotop H, Illenberger E, Morgner H, Niehaus A (1971) Chem Phys Lett 10:493
72. Bruna PJ, Peyerimhoff SD (1987) Adv Chem Phys 87:1
73. Theodorakopoulos G, Petsalakis ID (1988) Chem Phys Lett 149:196
74. Petsalakis ID, Theodorakopoulos G, Consta S (1992) Mol Phys 75:805
75. Petsalakis ID, Theodorakopoulos G (1994) J Phys B 27:4483
76. Zemke WT, Olson RE, Verma KK, Stwalley WC, Liu B (1984) J Chem Phys 80:356
77. Rich WG, Bobbio SM, Champion RL, Doverspike LD (1971) Phys Rev A 4:2253
78. Mittmann H-U, Weise H-P, Ding A, Henglein A (1971) Z Naturforsch Teil A 26:1112
79. Weise H-P, Mittmann H-U, Ding A, Henglein A (1971) Z Naturforsch Teil A 26:1122
80. Klingbeil R (1972) J Chem Phys 57:1066
81. Gianturco FA, Niedner G, Noll M, Semprini E, Stefani F, Toennies JP (1987) Z Phys D 7:281
82. Gianturco FA, Patriarca M (1989) Nuovo Cimento D 11:1287
83. Baer M, Düren R, Friedrich B, Niedner G, Noll M, Toennies JP (1987) Phys Rev A 36:1063
84. Julienne PS, Smith AM, Burnett K (1993) Adv At Mol Opt Phys 30:141
85. Haberland H, Lee YT, Siska PE (1981) Adv Chem Phys 45:487
86. Haberland H, Weber W (1980) J Phys B 13:4147
87. Way KR, Stwalley WC (1973) J Chem Phys 59:5298
88. Buck U, Hoppe HO, Huisken F, Pauly H (1974) J Chem Phys 60:4925